Med Glas (Zenica)

Medicinski Glasnik

ISSN 1840-2445 (Online); ISSN 1840-0132 (Print)

Medical Association of Zenica-Doboj Canton

Included by: PubMed (MEDLINE), SCOPUS, EMBASE, CNKI and DOAJ.

Type of the paper:	**ORIGINAL ARTICLE**
Running title:	**Hasson et al.** Antibiotic-associated *E. coli* motion dynamics
Title:	**Mechanical motion dynamics of surface-adhered *Escherichia coli* exposed to ampicillin and polymyxin B: an exploratory computational analysis**
Authors:	Rasha Nazar Hasson[1], Rana Ibrahim Al-Sabaawi[1], Mahmood Abduljabar Altobje[2*]
Affiliations:	[1]Department of Biology, College of Education for Women, University of Mosul, Mosul, Iraq; [2]Department of Biology, College of Science, University of Mosul, Mosul, Iraq
Corresponding author:	Mahmood Abduljabar Altobje, Department of Biology, College of Science, University of Mosul, Main Cultural Complex Street, Mosul 41002, Iraq Phone: +964 770 187 1611 E-mail: mahmoodaltobje1967@gmail.com
DOI:	https://doi.org/10.17392/medglas24742

Received: 28 April 2026
Revised: 30 July 2026
Accepted: 05 August 2026

ORIGINAL ARTICLE

Mechanical motion dynamics of surface-adhered *Escherichia coli* exposed to ampicillin and polymyxin B: an exploratory computational analysis

Rasha Nazar Hasson[1], Rana Ibrahim Al-Sabaawi[1], Mahmood Abduljabar Altobje[2*]

[1]Department of Biology, College of Education for Women, University of Mosul, Mosul, Iraq;

[2]Department of Biology, College of Science, University of Mosul, Mosul, Iraq

Running title: Hasson et al. Antibiotic-associated *E. coli* motion dynamics

***Correspondence:**

Mahmood Abduljabar Altobje

Department of Biology, College of Science, University of Mosul,

Main Cultural Complex Street, Mosul 41002, Iraq

Phone: +964 770 187 1611

Email: mahmoodaltobje1967@gmail.com

ORCID ID: 0000-0002-0507-4469

ABSTRACT

Aim: To explore whether motion features extracted from publicly available supplementary recordings distinguish the responses of surface-adhered *Escherichia coli* HCB136 to ampicillin and polymyxin B using Gaussian mixture models (GMMs) and Gaussian process regression (GPR).

Methods: This secondary computational analysis included all seven supplementary recordings published by Johnson et al. (2017): three polymyxin B and four ampicillin recordings of non-motile *E. coli* K-12 HCB136 with paralysed flagella adhered to quartz resonators. Motion features were extracted using optical-flow and centroid-tracking procedures and explored using GMMs, principal component analysis, K-means clustering, video-level linear trends, and GPR.

Results: Normalised motion decreased by 93–98% in the polymyxin B recordings and by 50–62% in the ampicillin recordings. Polymyxin B recordings showed lower and less dispersed GMM-derived motion features, whereas ampicillin recordings showed greater between-recording variability. Descriptive temporal profiles showed distinct patterns, but independent predictive validation was not possible.

Conclusion: The available recordings under the two antibiotic conditions showed different mechanical motion patterns in this secondary analysis. Because only seven publicly available recordings from one strain and one concentration of each antibiotic were analysed, the findings are exploratory and require validation against standard antimicrobial susceptibility endpoints.

Keywords: ampicillin; *Escherichia coli*; models, statistical; polymyxin B

INTRODUCTION

Bacterial mechanical motion can reflect physiological activity and stress responses before changes in population growth become apparent. Conventional antimicrobial susceptibility methods primarily assess growth inhibition or viability, whereas imaging and nanomotion approaches quantify early physical changes in individual cells or surface-adhered populations (1–3). These approaches may provide complementary information, although their analytical validity and relationship to established susceptibility endpoints require careful evaluation.

Antibiotics with different mechanisms of action can produce distinct temporal responses. Beta-lactams such as ampicillin inhibit peptidoglycan synthesis and may produce delayed morphological disruption, whereas polymyxin B rapidly alters the Gram-negative cell envelope (3–5). Mechanical and optical signals have therefore been investigated as potential early indicators of antibiotic exposure (1–3). Bacterial motility can also influence adaptation in spatially heterogeneous antibiotic environments (6).

Gaussian mixture models (GMMs) classify observations into latent components without prespecified thresholds, while Gaussian process regression (GPR) provides a probabilistic framework for modelling non-linear temporal trajectories and uncertainty. Gaussian processes have been used to model microbial growth and stress responses (7,8), but their combined use with mixture models for video-based bacterial motion phenotyping remains insufficiently characterised.

The combined use of discrete and continuous motion models raises important methodological issues, including definition of the experimental unit, independence of recording-derived observations, reproducibility across biological replicates, and validation against conventional antimicrobial susceptibility testing.

This study aimed to characterise motion features in publicly available recordings of surface-adhered *E. coli* HCB136 exposed to ampicillin or polymyxin B and to examine whether GMM- and GPR-derived summaries distinguish the resulting temporal patterns.

MATERIAL AND METHODS

Material and study design

This secondary computational analysis used all seven supplementary recordings published by Johnson et al. (2017) under a Creative Commons Attribution 4.0 licence: three polymyxin B recordings and four ampicillin recordings. No new bacterial cultures, antibiotic exposures, imaging, or laboratory measurements were performed.

In the original experiment, non-motile *Escherichia coli* K-12 HCB136 with paralysed flagella was grown in lysogeny broth at 37 °C with agitation. Cultures were diluted 1:500, incubated to an optical density at 600 nm (OD_{600}) of approximately 0.05, concentrated by filtration, and resuspended to OD_{600} 0.36 ± 0.02. Cells were adhered to poly-L-lysine-coated quartz-crystal resonators and exposed to ampicillin 100 µg/mL or polymyxin B 200 µg/mL. The AT-cut resonators had an approximately 5 MHz fundamental frequency, a diameter of 14 mm, and gold electrodes, and were coated with 200 µL of 0.01% poly-L-lysine for 5 minutes. Full experimental details are available in the source publication (3).

Methods

The source recordings were acquired with a 50× objective (numerical aperture 0.55) and a 1392 × 1040-pixel, 12-bit greyscale camera over a 178 × 133 µm field. The supplementary files included a compiled time-lapse sequence assembled from images acquired at approximately 1-minute intervals and short real-time clips recorded for 20 seconds at 6 frames/s. Images underwent background subtraction, greyscale normalisation, and Otsu binary segmentation.

Custom Python scripts applied optical-flow and centroid-tracking procedures to estimate cell-cluster displacement over time. Frame-level displacement vectors were aggregated into a motion-intensity series for each recording. Each series was normalised to its own pre-exposure baseline, which was set to 1.00; post-exposure values were expressed relative to that baseline. The post-exposure value reported in Table 1 represents the recording-level normalised value derived from the corresponding post-exposure motion series; values were not pooled across recordings. All seven publicly available recordings were included and treated as descriptive analytical units because the number of independent cultures, resonators, and fields of view could not be fully reconstructed from the source files.

A combined analytical pipeline was used to summarise motion states with Gaussian mixture models (GMMs) and temporal trajectories with Gaussian process regression (GPR).

For each recording, pixel-wise displacement vectors were calculated between successive frames using a custom optical-flow procedure. Motion magnitude $M(t)$ at time t was defined as:

$$M(t) = \frac{1}{N}\sum_{i=1}^{N}\sqrt{(x_i^{t+1} - x_i^t)^2 + (y_i^{t+1} - y_i^t)^2}$$

where N is the number of tracked pixels and (x, y) are the coordinates of pixel i at time t. This produced a time series $\{M(t)\}$ representing the mean motion intensity per frame.

A GMM was fitted to the distribution of motion magnitudes. The observed data $X = \{M(t)\}$ were assumed to arise from a mixture of K Gaussian components:

$$P(X) = \sum_{k=1}^{K} \pi_k \, \mathcal{N}(X \mid \mu_k, \Sigma_k)$$

Parameters were estimated using expectation–maximisation, and the number of components was selected using the Bayesian information criterion:

$$\mathrm{BIC} = -2\log(L) + q\log(n)$$

where L is the likelihood, q is the number of estimated parameters, and n is the number of observations. Component membership was interpreted as representing distinct statistical motion states.

GMM-derived motion features were used for descriptive multivariate analysis by principal component analysis (PCA) and K-means clustering. GMMs were fitted separately for the two antibiotic conditions, and the number of GMM components was selected using the Bayesian information criterion (BIC). The fitted component values formed the descriptive feature set used for PCA and K-means, and mean GMM component values were used as summaries of the fitted components. The plotted points in Figure 2 therefore represent GMM-derived observations rather than independent biological replicates. The available analysis record does not document additional feature scaling before PCA. The displayed K-means analysis used two clusters ($k = 2$), corresponding to the two clusters shown in Figure 2C. Because multiple observations could originate from the same recording, all multivariate results were interpreted descriptively and no confirmatory inference was performed.

GPR was used descriptively to model within-recording motion trajectories during antibiotic exposure. Motion observations were smoothed before model fitting to reduce transient spikes. A radial basis function (RBF) kernel was used, with hyperparameters optimised by grid search; the posterior predictive distribution was used to interpolate trajectories and estimate uncertainty. The numerical hyperparameter values and exact smoothing specification were not retained in the analysis record. Accordingly, GPR was interpreted qualitatively and no independent predictive validation was performed. The temporal profiles in Figure 4A and 4B are presented as descriptive motion trajectories rather than as standalone GPR performance outputs. Given the motion observations *M(t)*, the prior was defined as:

$$f(t) \sim \mathrm{GP}\big(0, k(t, t')\big)$$

A radial basis function kernel was used:

$$k(t, t') = \sigma_f^2 \exp\left[-\frac{(t - t')^2}{2\ell^2}\right]$$

where σ_f^2 is the signal variance and ℓ is the length scale. Hyperparameters were optimised by grid search. The posterior predictive distribution was used to interpolate the temporal trajectory and estimate uncertainty.

Statistical analysis

Analyses were implemented in Python using scikit-learn version 1.4.1. GMMs were fitted separately for the two antibiotic conditions. GPR was used descriptively to smooth and illustrate temporal trajectories. For each recording, a simple linear-regression slope of normalised motion across the within-recording temporal sequence was used as a descriptive trend index. Because the supplementary recordings had different temporal sampling structures, slope magnitude was not interpreted as a common physical rate or used for confirmatory comparison across recordings. Recording-level trends were classified descriptively as increasing or stable according to the fitted slope pattern shown in the analysis. Because only seven recordings were available and biological independence could not be established from the public files, no independent predictive validation or confirmatory inferential testing was performed.

RESULTS

All seven publicly available recordings were analysed: three from the polymyxin B condition and four from the ampicillin condition. Motion intensity was normalised within each recording to the corresponding pre-exposure baseline, set to 1.00. Post-exposure values were expressed relative to this baseline and are reported as recording-level normalised values.

Pre-exposure normalised motion was 1.00 in all seven recordings. After exposure, post-exposure motion values in the polymyxin B group were 0.05, 0.02, and 0.07, corresponding

to reductions of 95%, 98%, and 93%, respectively. The corresponding values in the ampicillin group were 0.45, 0.38, 0.50, and 0.42, corresponding to reductions of 55%, 62%, 50%, and 58%, respectively (Table 1, Figure 1).

Figure 2 shows descriptive GMM-based summaries. Mean GMM component values were lower and less dispersed in the polymyxin B group than in the ampicillin group (Figure 2A). Principal component analysis showed partial separation of the two antibiotic conditions, with limited overlap (Figure 2B). K-means clustering (k=2) yielded one dominant cluster containing most observations and one small cluster defined by a high-PC1 observation (Figure 2C). Because multiple plotted observations could originate from the same recording, these multivariate patterns were interpreted descriptively rather than as independent biological-replicate evidence.

Figure 3 presents recording-level temporal summaries. Three polymyxin B recordings and one ampicillin recording had low or near-zero trend slopes, whereas two ampicillin recordings had more positive slopes and one showed a slight negative slope (Figure 3A). Recordings classified as increasing had higher mean GMM component values than those classified as stable (Figure 3B). The slope-versus-mean plot showed higher and more dispersed values in the ampicillin condition (Figure 3C), and the violin plot showed a higher distribution of mean GMM-derived values in the ampicillin condition (Figure 3D). Because the recordings had different temporal structures, slope values were interpreted only as within-recording descriptive trend indices, not as directly comparable physical rates.

Figure 4 provides descriptive temporal and comparative motion summaries. In ampicillin recording 1, motion magnitudes ranged from 0.05 to 0.21 and declined markedly at 15–17.5 seconds (Figure 4A). In polymyxin B recording 1, values ranged from 0.29 to 0.93 and peaked at approximately 15 seconds before declining (Figure 4B). Panels A and B are interpreted as descriptive temporal profiles rather than standalone predictive GPR outputs.

Across all observations, the mean-versus-standard-deviation plot showed broader dispersion for ampicillin (Figure 4C), and the boxplots showed higher mean motion magnitude and greater variability in ampicillin than in polymyxin B (Figure 4D,E).

Unexposed control recordings were not available among the publicly available supplementary files and were therefore not analysed.

DISCUSSION

This analysis found different mechanical motion patterns in seven publicly available recordings of surface-adhered *E. coli* HCB136 exposed to ampicillin or polymyxin B. Polymyxin B was associated with larger reductions in normalised motion and less dispersed GMM-derived features, whereas ampicillin showed greater between-recording variability. These findings describe the available recordings and should not be interpreted as a validated comparison of antibiotic efficacy.

The observed temporal differences are biologically plausible because ampicillin disrupts cell-wall synthesis over time, whereas polymyxin B acts directly on the Gram-negative cell envelope (3,9,10). Previous nanomotion studies have shown that mechanical signals can change shortly after antibiotic exposure and may complement growth-based measurements (1–3).

GMM and GPR provided complementary exploratory summaries: GMM represented latent distributions of motion features, while GPR was used to describe non-linear trajectories. However, the biological meaning of the mixture components was not independently validated, and the source dataset did not support an independent assessment of predictive performance.

The main methodological contribution is the proposed combination of discrete and continuous models for exploratory motion phenotyping. Similar Gaussian-process methods

have been used to model microbial growth (7,8), but the present analysis requires validation using independent biological replicates before claims of classification or prediction can be supported.

The relationships between slopes and GMM-derived values should be interpreted with particular caution. With only three polymyxin B and four ampicillin recordings, the observed patterns are highly sensitive to individual recordings and do not constitute cross-model validation.

Motion-based measurements may eventually contribute to rapid phenotypic susceptibility testing, but clinical utility cannot be inferred from this study. Validation would require predefined inclusion criteria, multiple strains and antibiotic concentrations, comparison with minimum inhibitory concentration and reference antimicrobial susceptibility methods, and independent testing of resistant and susceptible isolates (2).

This study has several limitations. It was a secondary analysis of only seven publicly available recordings from one non-motile *E. coli* strain and one concentration of each antibiotic. The number of independent cultures, resonators, and control recordings could not be fully reconstructed from the source files, and multiple fields or frames from the same culture may not represent independent biological replicates. The study did not include dose–response experiments, minimum inhibitory concentration measurements, viability assays, or molecular markers of cellular injury. Exact computational reproducibility is additionally limited because the analysis record did not retain the named optical-flow implementation, any additional PCA scaling specification, the exact smoothing filter, or the numerical GPR hyperparameters. These limitations restrict reproducibility, mechanistic interpretation, and generalisability.

CONCLUSION

Recordings obtained under the ampicillin and polymyxin B conditions showed different mechanical motion patterns in surface-adhered *E. coli* HCB136. The combined GMM–GPR framework may be useful for exploratory motion phenotyping, but larger biologically replicated datasets, accessible code and data, dose–response assessment, and validation against standard antimicrobial susceptibility endpoints are required before diagnostic application can be considered.

Acknowledgements: The authors thank the College of Science, University of Mosul, for institutional support.

Funding: No external funding was received for this study.

Conflicts of interest: None to declare.

Author contributions (CRediT): Conceptualization—R.N.H. and M.A.A.; methodology—R.N.H., R.I.A.S., and M.A.A.; formal analysis—R.I.A.S.; investigation—R.N.H.; data curation—R.N.H. and R.I.A.S.; writing—original draft—M.A.A.; writing—review and editing—R.N.H., R.I.A.S., and M.A.A.; supervision—M.A.A.; project administration—M.A.A. All authors have read and agreed to the published version of the manuscript.

Ethics statement: Ethical and biosafety approval was not required because this study was a secondary computational analysis of publicly available experimental recordings and involved no new human, animal, or laboratory experimentation.

Data availability statement: The image sequences analysed in this study are the publicly available supplementary files accompanying Johnson et al. (Scientific Reports 2017;7:12138), distributed under a Creative Commons Attribution 4.0 International licence. The processed motion-feature matrix and analysis code generated for this study are available from the corresponding author on reasonable request.

REFERENCES

1. Kasas S, Malovichko A, Villalba MI, Vela ME, Yantorno O, Willaert RG. Nanomotion detection-based rapid antibiotic susceptibility testing. Antibiotics (Basel) 2021;10:287. doi: 10.3390/antibiotics10030287.

2. Sturm A, Jóźwiak G, Verge MP, Munch L, Cathomen G, Vocat A, et al. Accurate and rapid antibiotic susceptibility testing using a machine learning-assisted nanomotion technology platform. Nat Commun 2024;15:2037. doi: 10.1038/s41467-024-46213-y.

3. Johnson WL, France DC, Rentz NS, Cordell WT, Walls FL. Sensing bacterial vibrations and early response to antibiotics with phase noise of a resonant crystal. Sci Rep 2017;7:12138. doi: 10.1038/s41598-017-12063-6.

4. Meredith HR, Lopatkin AJ, Anderson DJ, You L. Bacterial temporal dynamics enable optimal design of antibiotic treatment. PLoS Comput Biol 2015;11:e1004201. doi: 10.1371/journal.pcbi.1004201.

5. Alikhani MS, Nazari M, Hatamkhani S. Enhancing antibiotic therapy through comprehensive pharmacokinetic/pharmacodynamic principles. Front Cell Infect Microbiol 2025;15:1521091. doi: 10.3389/fcimb.2025.1521091.

6. Piskovsky V, Oliveira NM. Bacterial motility can govern the dynamics of antibiotic resistance evolution. Nat Commun 2023;14:5584. doi: 10.1038/s41467-023-41196-8.

7. Tonner PD, Darnell CL, Engelhardt BE, Schmid AK. Detecting differential growth of microbial populations with Gaussian process regression. Genome Res 2017;27:320-33. doi: 10.1101/gr.210286.116.

8. Dharmawan K, Ramona Y. Comparative analysis of Gaussian process regression, Richards model, and polynomial regression for modeling bacterial growth dynamics of *Proteus mirabilis*. Microbiol Biotechnol Lett 2025;53:198-205. doi: 10.48022/mbl.2501.01013.

9. Elshobary ME, Badawy NK, Ashraf Y, Zatioun AA, Masriya HH, Ammar MM, et al. Combating antibiotic resistance: mechanisms, multidrug-resistant pathogens, and novel therapeutic approaches: an updated review. Pharmaceuticals (Basel) 2025;18:402. doi: 10.3390/ph18030402.

10. Jiang Z, Fu L, Wei C, Fu Q, Pan S. Antibacterial micro/nanomotors: advancing biofilm research to support medical applications. J Nanobiotechnology 2023;21:388. doi: 10.1186/s12951-023-02162-0.

TABLES AND FIGURES

Table 1. Normalised bacterial motion before and after antibiotic exposure in the seven publicly available recordings

Video	Antibiotic	Pre-exposure normalised motion	Post-exposure normalised motion	Reduction (%)
Video 1	PMB	1.00	0.05	95
Video 2	PMB	1.00	0.02	98
Video 3	PMB	1.00	0.07	93
Video 1	Ampicillin	1.00	0.45	55
Video 2	Ampicillin	1.00	0.38	62
Video 3	Ampicillin	1.00	0.50	50
Video 4	Ampicillin	1.00	0.42	58

PMB, polymyxin B.

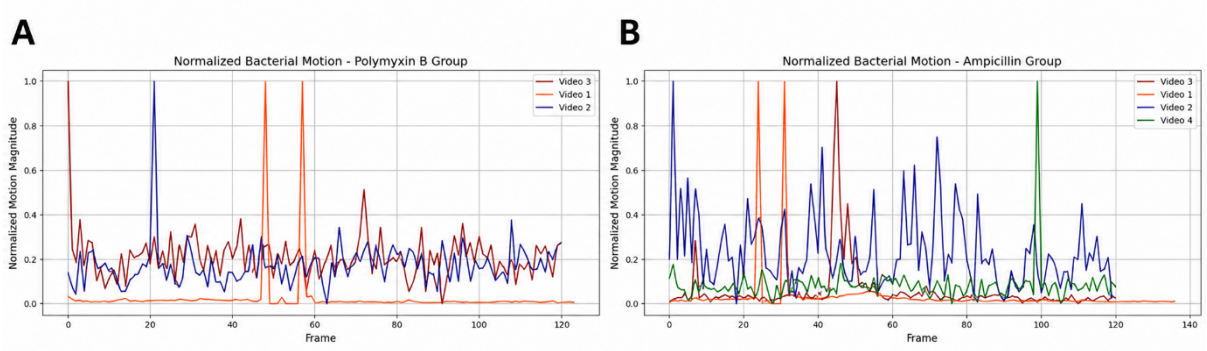

Figure 1. Normalised bacterial motion over time for *E. coli* exposed to (A) polymyxin B and (B) ampicillin.
PMB, polymyxin B.

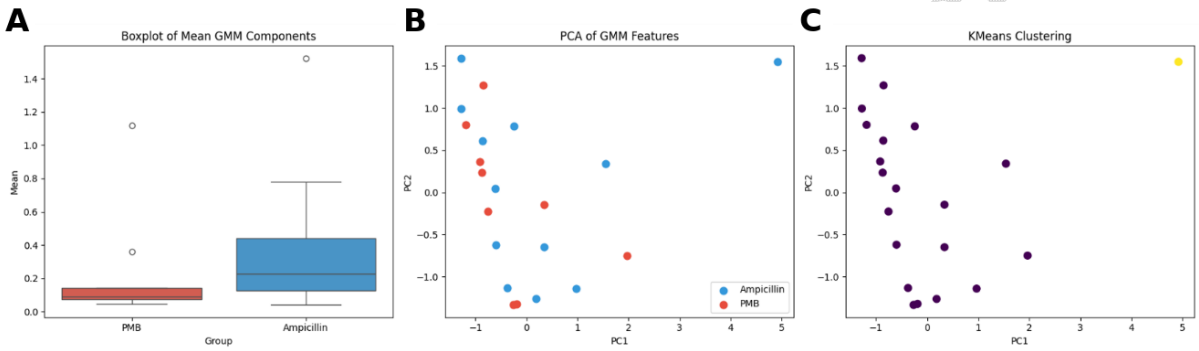

Figure 2. Descriptive multivariate summaries of Gaussian mixture model (GMM)-derived motion features by antibiotic condition: (A) distribution of mean GMM component values by antibiotic condition; (B) principal component analysis of GMM-derived observations; and (C) K-means clustering of GMM-derived observations.
GMM, Gaussian mixture model; PC, principal component; PCA, principal component analysis; PMB, polymyxin B. The K-means panel displays $k = 2$ clusters.

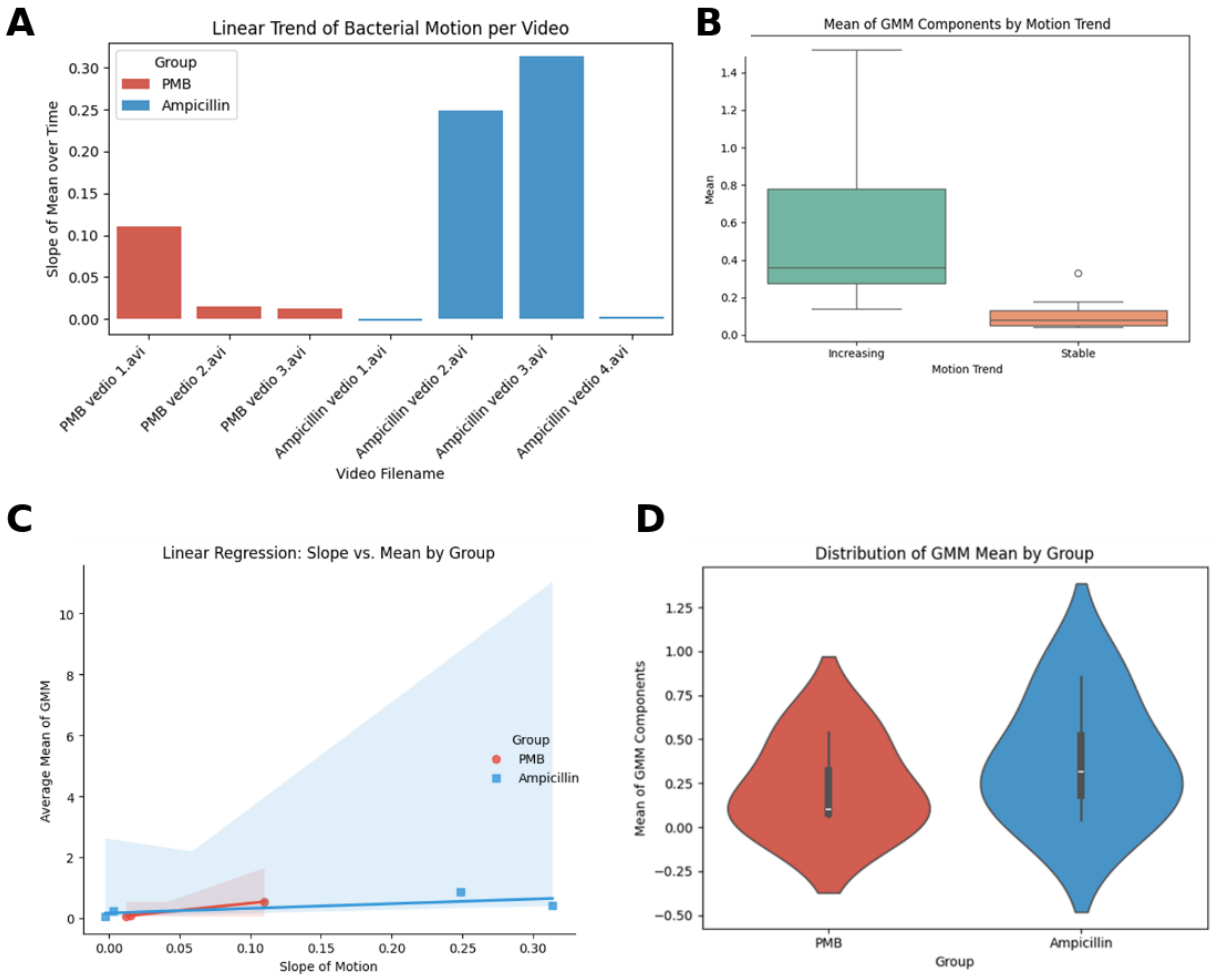

Figure 3. Descriptive recording-level temporal-trend and Gaussian mixture model (GMM) summaries by recording and antibiotic condition: (A) linear-regression trend slope for each recording; (B) distribution of mean GMM component values by motion-trend category; (C) relationship between motion slope and mean GMM-derived value by antibiotic condition; and (D) distribution of mean GMM-derived values by antibiotic condition.

GMM, Gaussian mixture model; PMB, polymyxin B. Trend slopes are within-recording descriptive indices and are not interpreted as common physical rates across recordings with different temporal sampling structures.

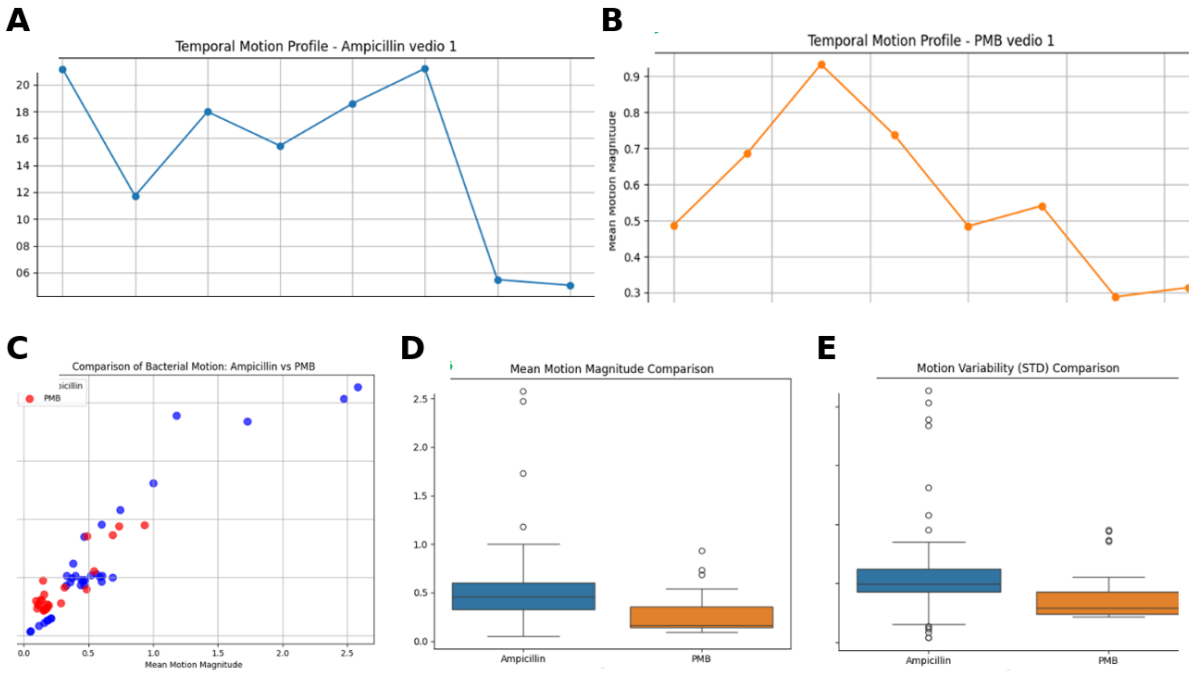

Figure 4. Descriptive temporal and comparative motion summaries: (A) temporal profile of ampicillin recording 1, (B) temporal profile of polymyxin B recording 1, (C) mean motion magnitude plotted against motion variability, (D) distribution of mean motion magnitude by antibiotic condition, and (E) distribution of motion variability by antibiotic condition.

GPR, Gaussian process regression; PMB, polymyxin B; STD, standard deviation. Panels A and B are presented as descriptive motion trajectories rather than standalone GPR performance outputs.